doi:10.1006/jmbi.2000.3791 available online at http://www.idealibrary.com on IDEAL® *J. Mol. Biol.* (2000) **299**, 1313–1324

JMB

The Free Yeast Aspartyl-tRNA Synthetase Differs from the tRNA^{Asp}-complexed Enzyme by Structural Changes in the Catalytic Site, Hinge Region, and Anticodon-binding Domain

Claude Sauter[1], Bernard Lorber[1], Jean Cavarelli[2], Dino Moras[2] and Richard Giegé[1]*

[1]*Département Mécanismes et Macromolécules de la Synthèse Protéique et Cristallogenèse UPR 9002, Institut de Biologie Moléculaire et Cellulaire du CNRS, 15 rue René Descartes 67084 Strasbourg Cedex France*

[2]*UPR 9004, Institut de Génétique et de Biologie Moléculaire et Cellulaire, 1 rue Laurent Fries, 67404 Illkirch Cedex, France*

**Corresponding author*

Aminoacyl-tRNA synthetases catalyze the specific charging of amino acid residues on tRNAs. Accurate recognition of a tRNA by its synthetase is achieved through sequence and structural signalling. It has been shown that tRNAs undergo large conformational changes upon binding to enzymes, but little is known about the conformational rearrangements in tRNA-bound synthetases. To address this issue the crystal structure of the dimeric class II aspartyl-tRNA synthetase (AspRS) from yeast was solved in its free form and compared to that of the protein associated to the cognate tRNA^{Asp}. The use of an enzyme truncated in N terminus improved the crystal quality and allowed us to solve and refine the structure of free AspRS at 2.3 Å resolution. For the first time, snapshots are available for the different macromolecular states belonging to the same tRNA aminoacylation system, comprising the free forms for tRNA and enzyme, and their complex. Overall, the synthetase is less affected by the association than the tRNA, although significant local changes occur. They concern a rotation of the anticodon binding domain and a movement in the hinge region which connects the anticodon binding and active-site domains in the AspRS subunit. The most dramatic differences are observed in two evolutionary conserved loops. Both are in the neighborhood of the catalytic site and are of importance for ligand binding. The combination of this structural analysis with mutagenesis and enzymology data points to a tRNA binding process that starts by a recognition event between the tRNA anticodon loop and the synthetase anticodon binding module.

Keywords: crystallographic structure; aspartyl-tRNA synthetase; yeast; free enzyme

Introduction

Aminoacyl-tRNA synthetases (aaRSs) catalyze the first step in protein synthesis. They are responsible for the fixation of amino acid residues to the cognate tRNA molecules (Arnez & Moras, 1997; Carter Jr, 1993; Lapointe & Giegé, 1991; Meinnel *et al*., 1995). In general, every living cell contains 20 aaRSs, and each synthetase is specific for one amino acid residue and its cognate tRNA family. Nevertheless, a few organisms are known where two aaRSs co-exist for the same amino acid specificity (e.g. LysRS in *Escherichia coli* (Lévêque *et al*., 1990) or AspRS in *Thermus thermophilus* (Becker *et al*., 1997)), or where certain aaRSs are missing, i.e. GlnRS in many bacteria and organelles (Gagnon *et al*., 1996; Lamour *et al*., 1994). Based on the sequence and the structure of their catalytic site, aaRSs have been ranked in two classes (Cusack *et al*., 1990; Eriani *et al*., 1990). In both classes, tRNA aminoacylation takes place in two steps: the amino acid residue is first activated in the presence of ATP and magnesium to form an

Abbreviations used: AspRS, aspartyl-tRNA synthetase; AspRS-70, truncated AspRS; aaRS, aminoacyl-tRNA synthetase with aa the amino acid residue in the three letter code.

E-mail address of the corresponding author: R.Giege@ibmc.u-strasbg.fr

0022-2836/00/051313–12 $35.00/0

aminoacyl-adenylate; then the amino acid moiety is transferred to the 3′-end of the tRNA (for a review, see First, 1998). The correct translation of the genetic code, therefore, relies on the accuracy of ligand recognition by the synthetases (Söll & RajBhandary, 1995) and of optimized reaction kinetics (First, 1998; Ibba *et al*., 1999).

The aspartate system offers a detailed description of the different states that exist for an aminoacylation system of class II synthetases. A series of crystallographic structures have been solved over the last two decades, starting with the free $tRNA^{Asp}$ from yeast (Moras *et al*., 1980) and its binary complex with AspRS (Cavarelli *et al*., 1993; Ruff *et al*., 1991). The binding of the small ligands ATP-Mg^{2+} and L-Asp was investigated in the presence of the tRNA in the yeast and *E. coli* systems (Cavarelli *et al*., 1994; Eiler *et al*., 1999). It was also studied in the absence of the tRNA for the *T. thermophilus* enzyme (Poterszman *et al*., 1994) and, more recently, for the AspRS from *Pyrococcus kodakaraensis* KOD1 (Schmitt *et al*., 1998). The comparison of different states for this archeal protein highlighted a key-and-lock association mode for the residue; molecular dynamics suggested that this feature is sufficient to discriminate L-Asp from L-Asn (Archontis *et al*., 1998).

In the case of the yeast aspartate system, the comparison of the free and the bound state of $tRNA^{Asp}$ sheds light on the large conformational changes affecting its structure as a result of the interaction with the enzyme. The overall L-shape of the tRNA is conserved, but large modifications bring the two arms closer together (Ruff *et al*., 1991). Furthermore, an important conformational change in the anticodon loop facilitates its recognition by the synthetase (Cavarelli *et al*., 1993; Rees *et al*., 1996). Finally, the binding of ATP, magnesium and L-Asp in the catalytic site is known from the analysis of the crystal structures of AspRS-$tRNA^{Asp}$ complexes in the presence of the small ligands (Cavarelli *et al*., 1994). However, a comparison between the substrate-bound AspRS and the free enzyme is missing, because of difficulties encountered in the preparation of good quality crystals, as it is the case for aminoacylation systems of other specificities. Recently, crystals of yeast AspRS suitable for a crystallographic study were prepared (Sauter *et al*., 1999) and the structure determination of this enzyme in its free state became possible. Here, we report the X-ray structure of this free yeast AspRS at a resolution of 2.3 Å and describe the structural modifications it undergoes upon tRNA binding.

Results and Discussion

The crystalline enzyme

Although the first crystals of yeast AspRS were obtained long ago (Dietrich *et al*., 1980) their quality was always inadequate because of an anisotropic diffraction and a low resolution limit. This poor crystallizability of the native enzyme is correlated with the structural heterogeneity of the protein extracted from yeast cells, which is a mixture of polypeptide chains starting between residues 14 and 33 (Lorber *et al*., 1987, 1988) (Figure 1). The N-terminal heterogeneity, however, does not hamper crystallization of the complex with $tRNA^{Asp}$ (Giegé *et al*., 1980; Lorber *et al*., 1983; Ruff *et al*., 1988). Further biochemical experiments indicate that the 70 first residues are not required for the catalytic activity (Eriani *et al*., 1991; Lorber *et al*., 1988) and crystallography showed that the heterogeneous N-terminal extension of the protein remains disordered in the AspRS-$tRNA^{Asp}$ complex (Cavarelli *et al*., 1994; Ruff *et al*., 1991). For these reasons, an AspRS variant lacking its first 70 N-terminal residues (AspRS-70) was retained for crystallization. A tetragonal and a trigonal crystal form were obtained as the result of a rational search of crystallization conditions at low-protein supersaturation in a crystal-solution phase diagram

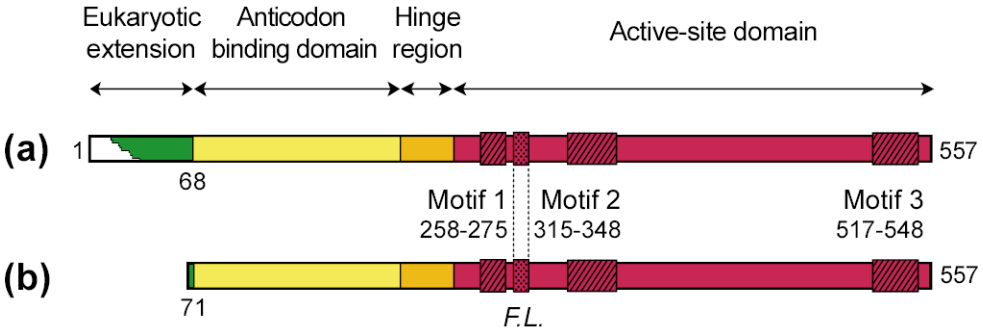

Figure 1. Primary structure of yeast AspRS and its modular organization in (a) the native, and (b) the truncated enzyme. The yeast AspRS gene (APS) codes for a monomer of 557 amino acid residues containing three structural domains in the AspRS monomer: the anticodon binding domain in the N terminus (yellow), the hinge region (orange), and the active-site domain in the C terminus (red) carrying three class II consensus sequence motives and the ''flipping loop'' (FL, for details, see the text). In AspRS purified from yeast (a), the N-terminal region (green) is heterogeneous and has been removed in (b) AspRS-70 which was used for this study. For cloning reasons, residues 14 to 17 from the native sequence (green) were linked to the N terminus of the 71-557 sequence.

(Sauter *et al*., 1999). We note that the crystalline enzyme lacking the N-terminal extension possesses otherwise exactly the same sequence as the native protein, except for the first four residues (67 to 70), which correspond to amino acid residues 14 to 17, shifted for cloning reasons (Vincendon, 1990).

Crystallographic aspects

The structure of AspRS-70 (for simplicity it is named AspRS below) was solved by molecular replacement (see Material and Methods). Data collected for trigonal crystals (space group $P3_221$) resulted in electron density maps of rather poor quality at medium resolution (~3.5 Å), due to a characteristic diffraction anisotropy. However, they allowed us to trace a C^{α} backbone for the dimer (results not shown), but further modeling and refinement remained unsuccessful. In contrast, the tetragonal crystal form (space group $P4_12_12$) provided an isotropic diffraction, even at high resolution (2.3 Å), and the initial density maps were of good quality.

The crystallographic data indicate a fully symmetric organization of the AspRS dimer, with one polypeptide chain in the asymmetric unit. The model was built and refined at 2.3 Å resolution to a *R*-factor of 20.2 % and a R_{free} of 24.2 % using standard methods (see Table 1). It encompasses residues 71 to 557 from the AspRS monomer (the four N-terminal residues could not be clearly located in the electron density map) and 227 ordered water molecules. Figure 2 gives an example of the electron density map in the region of the active-site core. This map was straightforwardly interpreted and clearly shows the five central anti-parallel β-strands that form the conserved framework for the catalytic domain of class II synthetases.

In the crystalline lattice, one intermolecular contact is of particular interest. It involves the loop 145 to 147 from the anticodon binding domain adjacent to the N terminus, and a external loop (495 to 500) located on the left-hand side of the active-site module of a neighboring monomer. The enhancement of the diffraction limit for the tetragonal crystals suggests that shortening the enzyme at its N terminus has favored this contact. Conversely, with the longer and heterogeneous AspRS extracted from yeast, this packing contact is hindered, and the crystals are of poor quality. We recall that the latter crystals belonged to the same space group, had identical cell parameters to those used here, but were highly anisotropic in diffraction (Dietrich *et al*., 1980).

Table 1. Data collection and refinement statistics

A. *X-ray data collection*	
Space group	$P4_12_12$
Unit cell lengths (Å)	$a = 90.23$, $c = 184.9$
Synchrotron beamline	ID14/EH4 (ESRF)
Resolution (Å)	20-2.3
Completeness (%)	98.2 (99.3)[a]
No. of observations	183,874
No. of unique reflections	34,124
Redundancy	5.4
R_{sym} (%)[b] and average ($I/\sigma(I)$)	8.2 (27.7)[a], 12 (4.6)[a]
B. *Refinement statistics*	
Refinement program	CNS
No. of reflections in working set	30,538
No. of reflections in test set	2299
R^{c}_{model}, R_{free} (%)	20.2, 24.2
Number of protein atoms	3944
Number of ordered water molecules	227
r.m.s.d. from ideal geometry	
Bond lengths (Å) and valence angles (deg.)	0.009, 1.47
Average *B*-factors for protein, water molecules (Å^2)	40.7, 43.4
Ramachandran plot quality[d]	
Residues in core, allowed, generously allowed regions (%)	91, 8.3, 0.7
Overall *G*-factor[d]	0.28

[a] The values in parentheses correspond to the highest resolution shell (2.3-2.35 Å).

[b] $R_{sym} = \Sigma_h \ \Sigma_i |\langle I_h \rangle - I_{h,i}| / \Sigma_h \ \Sigma_i \ I_{h,i}$ where $I_{h,i}$ is the *i*th observed intensity of reflection *h* and $\langle I_h \rangle$ the average intensity for this unique reflection.

[c] $R_{model} = \Sigma_h |F_{obs} - F_{calc}| / \Sigma_h \ F_{obs}$ where F_{obs} and F_{calc} are the observed and calculated structure factor amplitude, respectively.

[d] Calculated with PROCHECK.

General structural features of the free aspartyl-tRNA synthetase from yeast

The general organization of the free AspRS is illustrated Figure 3. The dimer has an elongated form of ~100 Å × 80 Å × 30 Å with a gyration radius of 31 Å. Each subunit of the dimer is made of three modules (Figure 3(a)): (i) the anticodon binding domain in the N terminus; (ii) a short hinge region (residues 205 to 240); and (iii) the active-site domain in C terminus. The structural organization (Figure 3(b), left) is identical to that of the enzyme associated to the tRNA, with the characteristic secondary structure features of subclass IIb synthetases, namely the anticodon binding domain formed by a five-stranded β-barrel with an OB fold (for oligomer binding fold) and the active-site domain built on a seven-stranded β-sheet (partly shown in Figure 2). These features are present in prokaryotic AspRSs (Delarue *et al*., 1994; Eiler *et al*., 1999; Schmitt *et al*., 1998), and in two other members of the class IIb, LysRS (Onesti *et al*., 1995) and AsnRS (Berthet-Colominas *et al*., 1998). As anticipated, the amino acid residues interacting with the tRNA (Cavarelli *et al*., 1993) provide electropositive patches at the surface of the subunit (Figure 3(b), right).

The free AspRS *versus* the enzyme associated to $tRNA^{Asp}$

An overview

The structure of the synthetase associated to $tRNA^{Asp}$ was determined by Ruff *et al*. (1991) and Cavarelli *et al*. (1993), and later on as a ternary and

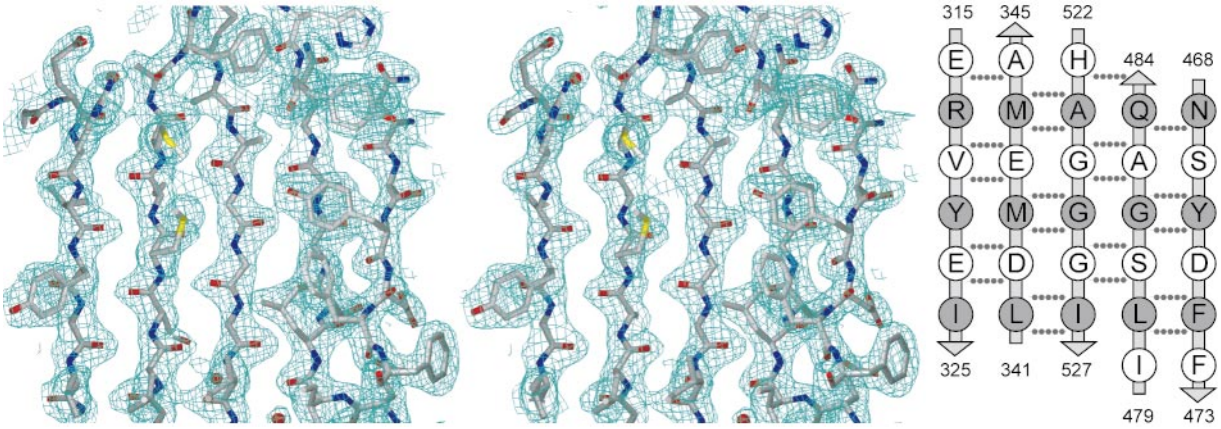

Figure 2. Stereoview of the electron density in the class II β-sheet region of the apo-enzyme active-site domain (from the left to the right, strands A2 to A6). The σ_a weighted $2mF_{obs} - DF_{calc}$ density was contoured at 1.3σ. The right panel gives a schematic representation of these five central β-strands with their orientation and sequence. Gray circles indicate amino acid residues with C^{α} atoms pointing toward the reader.

a quaternary complex containing ATP or aspartyl-adenylate, respectively (Cavarelli *et al.*, 1994). In each case, the two subunits were related by a non-crystallographic 2-fold axis and show faint differences. They will later be quoted as monomer A and B, as indicated in the PDB file (ID: 1asz). In order to calculate root mean square deviations (r.m.s.d.) on C^{α} positions, the free and the complexed monomers have been compared by least-square superposition of the core of their active-site module (i.e. the seven β-strands). Figure 4 superimposes the polypeptide chains of the free and bound AspRS subunits and highlights differences in various regions. The overall r.m.s.d. between the free subunit and monomers A and B are 1.4 and 1.2 Å, respectively. The deviations calculated for each

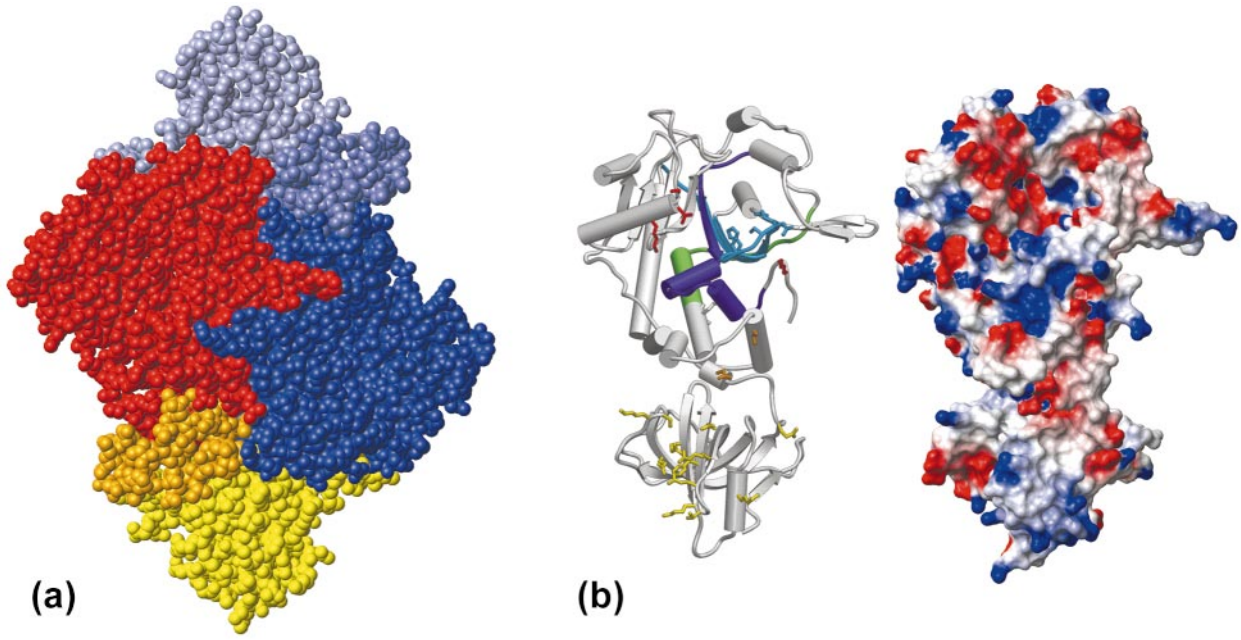

Figure 3. The free form of yeast AspRS. (a) The free dimer is shown with its 2-fold axis perpendicular to the figure. The three domains are represented in the left subunit using the same color code as described in the legend to Figure 1: the anticodon binding domain in yellow (light blue in the right monomer), the hinge region in orange (medium blue), and the active-site domain in red (dark blue). (b) The free AspRS monomer. On the left, the secondary structure elements determined with PROCHECK (Laskowsky *et al.*, 1993). The consensus sequence motives 1, 2 and 3 characteristic of class II synthetases are indicated in green, blue and purple, respectively. Side-chains involved in tRNA binding (Cavarelli *et al.*, 1993) are drawn in the color of the domain (or the sequence motif) to which they belong. On the right, the electrostatic potential at the surface of the monomer: electronegative regions are indicated in red and electropositive ones in blue.

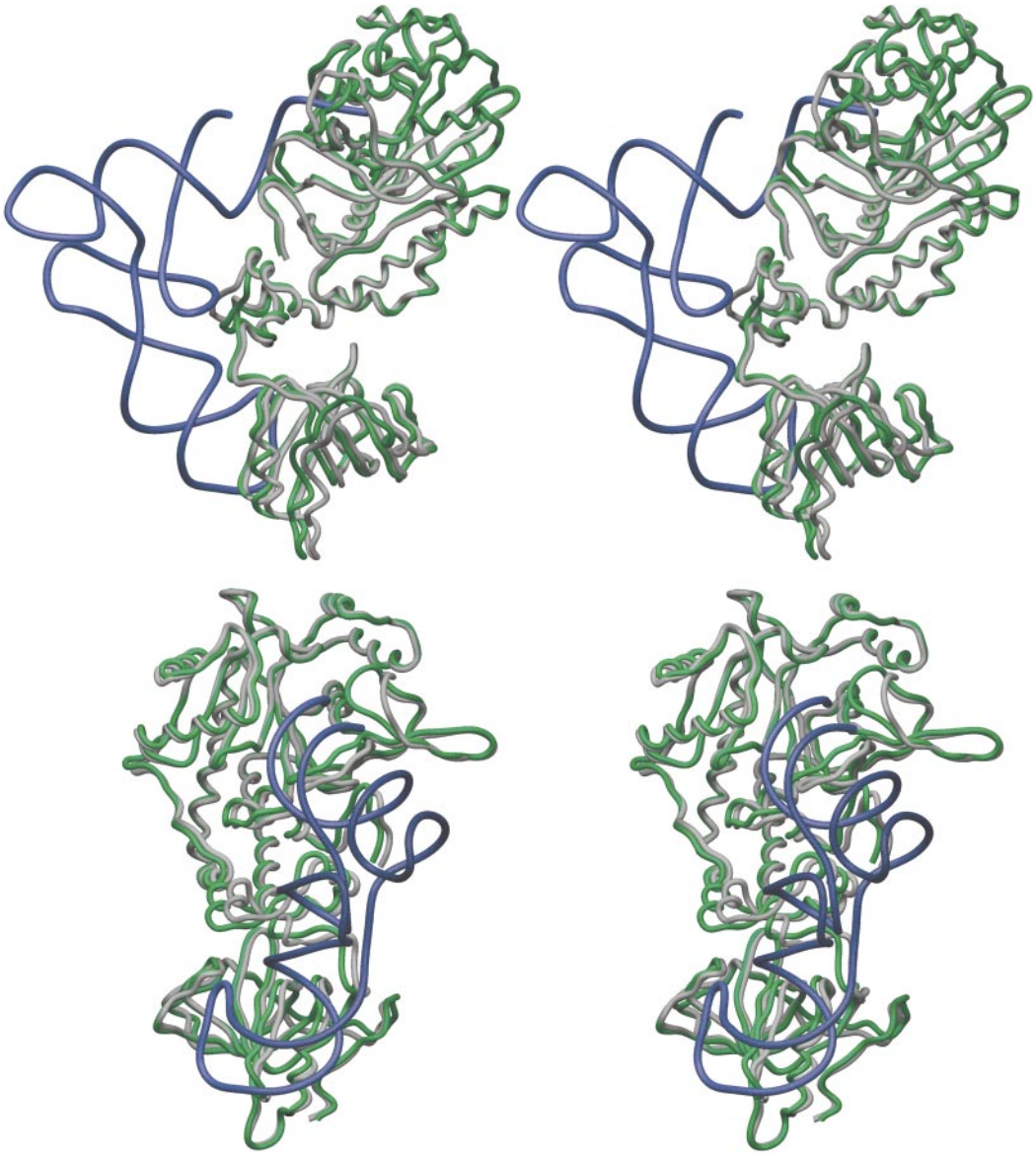

Figure 4. Comparison of free and tRNA bound AspRS subunits. The picture shows the free monomer (gray) superimposed to subunit B (green) in the complex with tRNA (blue). Monomers A and B in the structure of AspRS-ATP-$tRNA^{Asp}$ ternary complex are related by a non-crystallographic 2-fold axis (Cavarelli *et al.*, 1994). The two stereo views are turned by 90° with respect to each other. Monomers were superimposed by least squares minimization of the active-site seven stranded β-sheet (49 C^{α}).

module are indicated in Figure 5(a). Packing effects on the apo-enzyme conformation may be excluded since crystal contacts do not concern the regions pointed out below, such as the two mobile loops, which are both facing the solvent channels. In addition, the C^{α} backbone of the present tetragonal structure is very similar to that previously built from the trigonal data at lower resolution, including the conformation of the mobile loops surrounding the active site (results not shown).

The rotation of the anticodon binding domain

The N-terminal region forms the β-barrel that binds to the anticodon loop of the tRNA molecule (Cavarelli *et al.*, 1993). This part of the tRNA exhibits four identity elements: G34, U35, C36, and C38 (Frugier *et al.*, 1994b; Pütz *et al.*, 1991). During the transition from the free to the bound enzyme, this protein domain undergoes a rigid body movement corresponding to a rotation of ~6° with respect to the catalytic module (Figure 5(b)). The overall structure of the β-barrel is not affected. When the strands are superimposed independently from the rest of the monomers, their r.m.s.d. is not higher than 0.5 Å. Thus, similarly to the key-and-lock mechanism of anticodon binding observed in the *E. coli* system (Rees *et al.*, 2000), a weak adjustment of a few amino acid side-chains is sufficient to ensure, in a primary association event, the recognition of the identity nucleotides present in the tRNA anticodon loop.

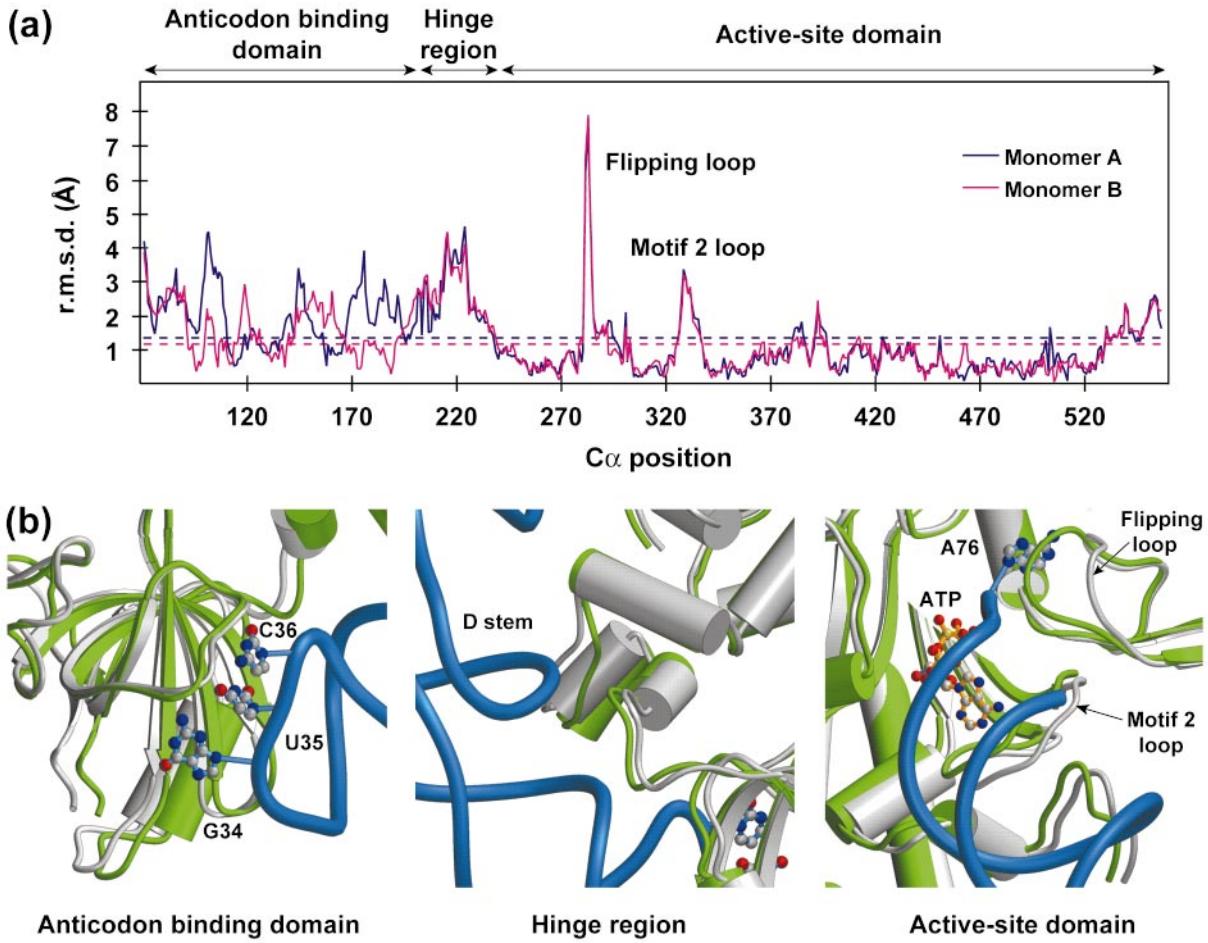

Figure 5. Movements in the AspRS monomers. (a) r.m.s.d. between free and tRNA bound subunits on C^{α} positions (calculated as described in the legend to Figure 4). Values are plotted in blue and red when the free subunit is compared to monomer A and B in the complex, respectively. The broken lines indicate the average r.m.s.d. value for the whole subunits. Average r.m.s.d. calculated for individual AspRS domains are 1.2 Å in the catalytic domain, 2.6 Å in the hinge region, 1.7 or 2.1 Å in the anticodon binding domain A or B (the latter values correspond to a rigid body rotation of this region of 6° and 6.4° in monomers A and B, respectively). (b) Close-up views for each of the three domains of the superimposed free subunit in gray and complex B monomer in green, with the bound tRNA in blue. The three anticodon bases are shown in interaction with the related protein module, as well as the ATP and the terminal nucleotide A76 bound in the active site.

The hinge region at a pivotal position

The hinge region formed by three helices is the smallest module in AspRS. It has a central location in the monomer and connects the two other domains of the protein. In the complex, it develops three interactions with the tRNA ribose-phosphate backbone at U11 and U12 in the D-stem (Cavarelli *et al*., 1993). When the catalytic cores are superimposed (Figure 5(b)), the hinge region of the free monomer is more external and prominent. In order to allow the binding of the D-stem, it moves backward toward the dimer gravity center. Values of r.m.s.d. indicate large variations in this zone (Figure 5(a)), mainly for the loop 205 to 218 and the following helix 220 to 230 containing the residues Asp210, Asp227, and Thr230, which contact the tRNA. Their movement may contribute to the re-orientation of the anticodon-binding domain, thus directing the tRNA so that its 3′-extremity comes into the catalytic groove.

Movements in the active site: a loop story

The structural variations in the active-site domain are limited (Figure 5(a)) except for two loops on the right-hand side of the catalytic groove (Figure 5(b)). The first one is the loop of motif 2 (Figures 1 and 5(b)) which contains highly conserved residues involved in the binding of ATP of the 3′-CCA end of the tRNA (Cavarelli *et al*., 1994; Eriani *et al*., 1995). The second loop is the so-called ''flipping loop'' (residues 279-285) which was already identified for its mobility in the AspRS structures from *T. thermophilus* and *P. kodakaraensis* (Moulinier, 1997; Schmitt *et al*., 1998). As with the prokaryotic apo-enzymes, both loops adopt an open conformation in the free yeast enzyme,

although the deviation is more pronounced in the flipping loop from yeast AspRS (e.g. r.m.s.d. values in this loop are less than 3 Å in *E. coli* (Rees *et al*., 2000), whereas they reach 8 Å in yeast (this paper)). In contrast, these loops interact with the tRNA 3′-accepting-end and with the small ligands in the yeast complex and contribute to the anchoring of the substrates in the catalytic cavity. Indeed, mutations in the residues which bind to the 3′-CCA display strong k_{cat} effects (Eriani & Gangloff, 1999) and site-directed mutagenesis confirmed their implication in the binding of the small ligands (Cavarelli *et al*., 1994). The situation is similar in the *E. coli* and *T. thermophilus* ternary complexes (Eiler *et al*., 1999; Moulinier, 1997). Furthermore, the structure of the *P. kodakaraensis* enzyme solved at 1.9 Å resolution, the highest resolution available to date for a synthetase, illustrates how these loops participate, independently from tRNA binding, in the process of formation and stabilization of the aminoacyl-adenylate (Schmitt *et al*., 1998). Here, we confirm the key role played by the loop of motif 2 and the flipping loop which are in an open position in the apo-enzyme and adopt various conformations depending on the ligand bound, through an induced-fit mechanism as described by Eiler *et al*. (1999). This situation can be generalized to the two other members of class IIb, LysRS (Onesti *et al*., 1995) and AsnRS (Berthet-Colominas *et al*., 1998) and maybe even to representatives of subclass IIa such as HisRSs, for which similar loop features have been described by Bovee *et al*. (1999) and Qiu *et al*. (1999).

A mutual structural adaptation

To achieve an accurate aminoacylation reaction, tRNAs and synthetases have developed sets of recognition signals. The latter include identity elements on tRNAs, mainly located in the anticodon loop and in the acceptor stem, that allow these molecules with a very similar 3D architecture to be distinguished each from the other (for a review, see Giegé *et al*., 1998b). These elements have counterparts on the synthetases, namely amino acid residues whose mutations strongly affect both tRNA binding and catalysis (e.g. Eriani & Gangloff, 1999). The specific recognition and efficient aminoacylation of a tRNA must actually imply structural changes and transconformations in both macromolecules in order to optimize the mutual fit. Crystallography has revealed such transconformations within complexed tRNAs (e.g. Rould *et al*., 1989; Ruff *et al*., 1991). The fact that synthetases are able to recognize a variety of RNA substrates is actually indicative of a certain degree of plasticity (Ebel *et al*., 1973; Giegé *et al*., 1998a) and the existence of transconformations within these enzymes is supported by indirect solution data (e.g. Zaccaï *et al*., 1979), but their exact nature remains elusive.

Having solved the respective structures of free synthetase and tRNA, and that of their complex, we can now consider the issue of the functioning of the aspartate system from yeast in a structural way. This study reveals the rather faint conformational changes at the level of the protein, with r.m.s.d. values on C^{α} positions of 1.2-1.4 Å. In comparison, the r.m.s.d. on the phosphate positions between the free tRNA (Moras *et al*., 1980; Westhof *et al*., 1985) and its bound form is 5.1 Å. This illustrates a drastic difference in flexibility and structural adaptability between the two macromolecules, as predicted by Rees *et al*. (1996), knowing the higher flexibility of the sugar-phosphate backbone. But at the local level in the synthetase, large conformational changes also occur with r.m.s.d. values of ~4 Å, with a maximum of 8 Å for the flipping loop (Figure 5(a)). Large-body movements in a monomer are restrained, likely because of the existence of the dimeric interface. Indeed, the oligomerization is a functional requirement and it was shown that AspRS subunits can communicate (cooperate) during the catalytic process (Eriani *et al*., 1993), even though the pathway has not yet been identified. On the other hand, the non-symmetric conformation of the catalytic domain in the two subunits of the complex (Ruff *et al*., 1991) is an additional argument for a cooperative functioning of the two AspRS subunits. Kinetic data favor this view (D. Kern, personal communication). Deciphering the molecular communication mechanism will probably become possible through a comparative analysis of the AspRSs from different organisms in various binding states. An analytic method is being developed for that purpose (L. Moulinier, personal communication).

A scenario for tRNA binding

Biochemical and structural data converge now toward a preferential sequence of events leading to the $tRNA^{Asp}$ binding onto AspRS (Figure 6). In this scenario, the synthetase first recognizes the tRNA by its anticodon loop (Figure 6(a)). The complementarity of the electropositive surfaces in the anticodon binding domain (Figure 3(b)) and the electronegative tRNA backbone may guide the association. Formation of the catalytically competent complex would then proceed by a mutual adaptation of both macromolecules, as reflected by the conformational differences between the free and complexed partners. In favor of the preponderant role of this protein domain is its structure ready to interact with the tRNA anticodon loop without any conformational change. A similar situation is observed in the *E. coli* system (Rees *et al*., 2000). The details of the recognition, however, remain to be deciphered, in particular, how bases in the tRNA anticodon loop unstack and adapt to the protein. Differences in aminoacylation efficiencies of $tRNA^{Asp}$ mimics confirm the importance of the anticodon loop in tRNA binding. Models for the interaction between the enzyme and two of these molecules are given in Figure 6(c). Thus, an anticodon stem-loop linked to a single-stranded

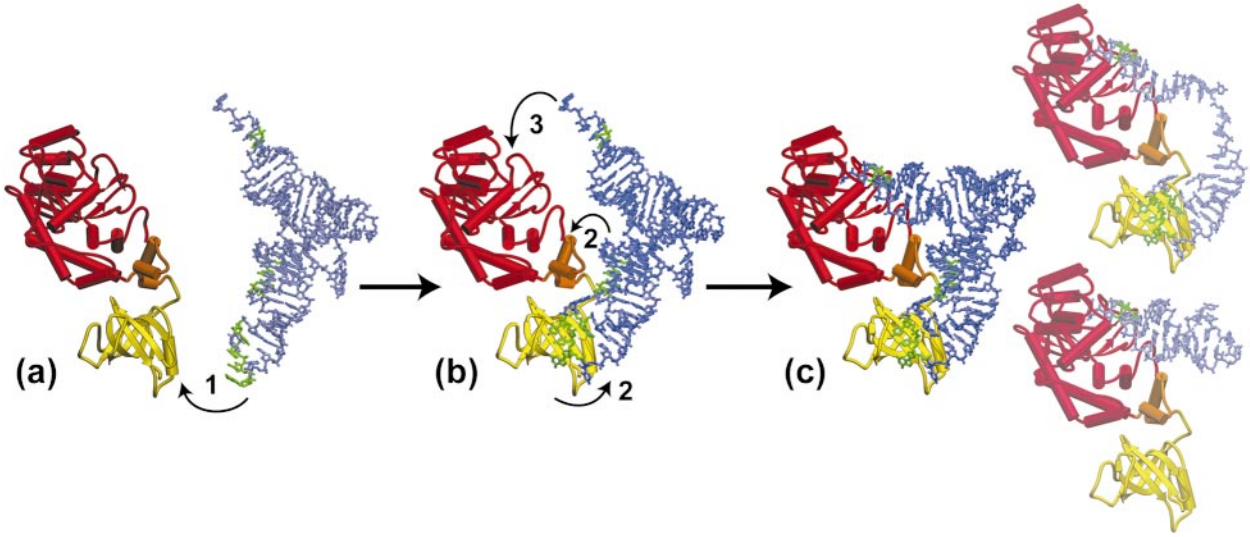

Figure 6. A structural representation of the recognition pathway of free AspRS by $tRNA^{Asp}$. (a) Free AspRS (*E*) (this work) and free $tRNA^{Asp}$ (*S*) (Moras *et al*., 1980; Westhof *et al*., 1985); (b) the putative intermediary partial complex between $tRNA^{Asp}$ and AspRS; (c) the active *ES* complex (Ruff *et al*., 1991) and models for the productive associations of AspRS with an RNA microhelix (Frugier *et al*., 1994a) and an anticodon stem-loop with a single-stranded acceptor-end (Wolfson *et al*., 1999). The tRNA recognizes first the synthetase through its anticodon loop (step 1), then the anticodon binding domain rotates and the hinge region interacts with the D-stem (step 2), finally the tRNA 3′-end enters the active site (step 3). In all structures, the active-site domain of AspRS monomers is kept in the same orientation and the color code for the three modules is the same as in Figures 1 and 2. Asp-tRNA identity nucleotides are indicated in green.

3′-acceptor-end is much better recognized (Wolfson *et al*., 1999) than a single minihelix restricted to the acceptor-end (Frugier *et al*., 1994a).

Recent mutagenesis studies indicate that specific contacts of AspRS with the anticodon triplet and the discriminator base of the tRNA constrain the complex so as to bring the acceptor stem into the active site (Eriani & Gangloff, 1999). They revealed that the main binding energy is provided by the anticodon binding module, as shown by mutations at 10 identified positions that trigger essentially K_d-effects and have only faint influences on k_{cat} values. Since the anticodon loop includes the major identity elements of $tRNA^{Asp}$ (Frugier *et al*., 1994b; Pütz *et al*., 1991), it can be concluded that the N-terminal module ensures both tRNA binding and tRNA selection (Figure 6(a)).

After the initial anchoring onto the N-terminal module of AspRS, the interaction might propagate through the hinge region which develops contacts with the D-stem (Figure 6(b)). Even though residues in the hinge area only bind the phosphate-ribose backbone of bases U11, U12 and G27 (Cavarelli *et al*., 1993), the specificity of these interactions is guided by the proximity of the G10:U25 identity base-pair (Pütz *et al*., 1991). Replacement of riboses of U11 and G27 by deoxyriboses prevents hydrogen bonding of 2′-hydroxyl groups and leads to a drastic loss of activity (Aphasizhev *et al*., 1997). Furthermore, mutations in the AspRS hinge region (Eriani & Gangloff, 1999) only affect the binding toward the catalytic center, where the major binding contributor is discriminator base G73. Altogether, this suggests a central role for the contacts between the hinge module in AspRS and the core region of tRNA during their mutual adaptation. The final step in adaptation occurs within the catalytic module of AspRS (Figure 6(b)), with the flipping and motif 2 loops in their closed conformation anchoring the tRNA acceptor-end in the catalytic site in an optimal position for aminoacylation (Figure 6(c)).

The above scenario is based on experimental data originating from studies with an active AspRS lacking its N-terminal extension entirely or partially. Recent investigations on the role of this 70 residue long extension indicate its participation in tRNA binding through additional contacts with the anticodon stem (Frugier *et al*., 2000). This confirms the preponderant role of the anticodon binding module of AspRS to which the extension is appended (Figure 1).

Concluding Remarks

Early investigations soon revealed the importance of the anticodon and the need of a mutual adaptation of tRNAs and synthetases for the formation of functional complexes, and phenomenological descriptions of this process were proposed (e.g. Ebel *et al*., 1979; Krauss *et al*., 1976). Today, the crystallographic data gained for the aspartate system allow for a structural description of complex formation at the molecular level. As perceived in the past, conformational changes in both tRNA and synthetase occur in a global induced-fit pro-

cess where the importance of anticodon loop binding to AspRS is highlighted. Although this study deals with a particular system, it is likely that similar conformational adaptations and binding modes (as in Figure 6) occur in other tRNA-synthetase systems. This is in particular the case in the *E. coli* aspartate system, where the anticodon, hinge and active site modules of AspRS undergo the same conformational changes upon binding of the cognate $tRNA^{Asp}$ (Rees *et al.*, 2000). We anticipate, however, that highest functional similarities will concern systems involving synthetases, closely related to AspRSs, as well as those where the strength of identity determinants in the anticodon is great. In agreement with this view are recent functional and structural data on class IIb human LysRS (Stello *et al.*, 1999) and on class IIa prokaryotic HisRSs (Bovee *et al.*, 1999; Qiu *et al.*, 1999). Likewise, specific binding of anticodon hairpins to aaRSs in anticodon dependent class I systems (e.g. Meinnel *et al.*, 1991) gives support to the rather general character of the scenario outlined in Figure 6. This scenario, that emphasizes the role of the anticodon binding module, is not in contradiction with the primordial role of the catalytic module in evolution and with the fact that this module can be activated, although not optimally, by minimalist tRNA structures (Schimmel *et al.*, 1993). Finally, the fact that AspRS can aspartylate a number of tRNA mimics with altered architecture indicates an elaborate adaptability of this protein in ligand binding. This functional plasticity confers selective advantage, since mutations within strategic positions in AspRS or tRNA will not necessarily inactivate the system.

Material and Methods

Crystallization and data collection

Crystals of yeast AspRS were grown from an enzyme lacking 70 residues in N terminus and purified from overproducing *E. coli* cells as described (Sauter *et al.*, 1999). Two crystal forms were obtained, tetragonal ($P4_12_12$) and trigonal ($P3_221$), and data sets were collected using synchrotron radiation at 2.95 and 3 Å resolution, respectively (Sauter *et al.*, 1999). A complete data set at 2.3 Å resolution was collected for the tetragonal form on the ID14/EH4 beamline at ESRF ($\lambda = 0.943$ Å) using a Quantum CCD detector. Data statistics are indicated in Table 1. The measurements were operated on a single crystal cooled at 110 K. Prior to flash-cooling, the crystal was soaked for 60 seconds in a mother liquor containing 20% (w/v) glycerol. Data were integrated with the HKL package (Otwinowski & Minor, 1997).

Molecular replacement and structure refinement

The structure was solved by molecular replacement using the coordinates of the yeast AspRS in the complex with the tRNA (Cavarelli *et al.*, 1994; Ruff *et al.*, 1991). By using the program AMoRe (Navaza & Saludjian, 1997), good packing solutions were found with one enzyme subunit per tetragonal asymmetric unit and a dimer in the trigonal unit (Sauter *et al.*, 1999). Despite good correlation and *R*-factor values with the trigonal data, many regions of the electron density map remained poorly defined in this space group, due to the characteristic anisotropy of trigonal crystals. The structure was therefore determined using the tetragonal crystals which provided an isotropic diffraction at a higher resolution.

The model of the free monomer was first refined against tetragonal crystallographic data at 2.95 Å (no sigma cut-off was applied) with CNS, using a cross-validated maximum likelihood crystallographic target and a bulk solvent correction (Brünger *et al.*, 1998). Stereochemical parameters were as described (Engh & Huber, 1991). The R_{free} value was calculated from a random sample containing 7.4% of the data (1124/15,190 reflections) in order to monitor the course of the refinement (Brünger, 1992). Rigid-body adjustment was performed, treating the three domains of the monomer separately, and this first step resulted in a *R*-factor of 43.4% ($R_{free} = 43.7$%). The model was adjusted by several cycles of graphic building and torsion angle dynamics and, after an individual *B*-factor refinement and the addition of 20 water molecules, the resulting *R*-factor was 21.8% and the R_{free} was 27.9%. The model was further refined using the second data set between 2.3-20 Å of resolution (see Table 1). In order to release any refinement memory in the new subset of reflections kept for R_{free} calculations (7.0% of the dataset), simulated annealing dynamics was performed at a high temperature. In the latest stage, Cartesian coordinate refinement was followed by individual *B*-factor refinement. Finally, water molecules developing sensible hydrogen bonds with protein or solvent atoms were added in $F_{obs} - F_{calc}$ difference density greater than 4σ.

The refined model

The final model consists of 487 residues corresponding to the amino acid residues 71 to 557 from the yeast AspRS monomer (the first four residues in N terminus are missing) and 227 water molecules. The crystallographic *R*-factor is 20.2% and R_{free} 24.2% for all reflections in the 2.3-20 Å resolution range. The model shows a good stereochemistry and geometry, as analyzed using the program PROCHECK (Laskowsky *et al.*, 1993) (Table 1). All residues have φ and ψ angles within the allowed regions of the Ramachandran plot, with 91% in the most favored region. The average *B*-factor of the model is 40.9 $Å^2$, in agreement with the overall *B*-factor determined by Wilson plot on diffraction data ($B = 39.7$ $Å^2$).

Structure modeling and comparison

Rebuilding and graphics operations were performed with the software O and, at every stage, models resulting from a refinement round were subjected to critical quality analyses using the program OOPS (Kleywegt & Jones, 1997). Superimposition of the free AspRS and the complex form and r.m.s.d. analyses were operated using O, CNS and LSQMAN (Kleywegt & Jones, 1997) as well as the modeling of AspRS/RNA complexes presented in Figure 6. In Figure 6(b), the free tRNA docked onto the apo-enzyme was constructed by transplanting the anticodon hairpin of the complexed tRNA (residues 29 to 41) into the free form, after superimposing the two tRNAs by their anticodon stem (r.m.s.d. = 1.1 Å for the phosphate groups). Figures were prepared with the programs SETOR and MOLMOL (Evans, 1993; Koradi *et al.*, 1996).

Accession Numbers

The atomic coordinates and structure-factor amplitudes have been deposited at the RCSB Protein Data Bank with the accession code 1eov.

Acknowledgments

We thank P. Auffinger, G. Eriani, M. Frugier, J. Gangloff, D. Kern, and B. Rees for discussion and critically reading the manuscript. We are deeply grateful to S. McSweeney and his team at ID14/EH4 beamline, ESRF-Grenoble, for their kind assistance during data collection. CS thanks the Association pour la Recherche sur le Cancer for a fellowship. This work was supported by CNRS, the EC (BIO4-CT98-0086 and BIO4-CT98-0189), CNES, and MENRT.

References

Aphasizhev, R., Théobald-Dietrich, A., Kostyuk, D., Kochetkov, S. N., Kisselev, L., Giegé, R. & Fasiolo, F. (1997). Structure and aminoacylation capacities of tRNA transcripts containing deoxyribonucleotides. *RNA,* **3**, 893-904.

Archontis, G., Simonson, T., Moras, D. & Karplus, M. (1998). Specific amino acid recognition by aspartyl-tRNA synthetase studied by free energy simulations. *J. Mol. Biol.* **275**, 823-846.

Arnez, J. & Moras, D. (1997). Structural and functional considerations of the aminoacylation reaction. *Trends Biochem. Sci.* **22**, 211-216.

Becker, H. D., Reinbolt, J., Kreutzer, R., Giegé, R. & Kern, D. (1997). Existence of two distinct aspartyl-tRNA synthetases in *Thermus thermophilus*. Structural and biochemical properties of the two enzymes. *Biochemistry,* **36**, 8785-8797.

Berthet-Colominas, C., Seignevert, L., Härtlein, M., Grotli, M., Cusack, S. & Leberman, R. (1998). The crystal structure of asparaginyl-tRNA synthetase from *Thermus thermophilus* and its complexes with ATP and asparaginyl-adenylate: the mechanism of discrimination between asparagine and aspartic acid. *EMBO J.* **17**, 2947-2960.

Bovee, M. L., Yan, W., Sproat, B. S. & Francklyn, C. S. (1999). tRNA discrimination at the binding step by a class II aminoacyl-tRNA synthetase. *Biochemistry,* **38**, 13725-13735.

Brünger, T. A. (1992). The free *R* value: a novel statistical quantity for assessing the accuracy of crystal structures. *Nature,* **355**, 472-474.

Brünger, A. T., Adams, P. D., Clore, G. M., DeLano, W. L., Gros, P., Grosse-Kunstleve, R. W., Jiang, J. S., Kuszewski, J., Nilges, M., Pannu, N. S., Read, R. J., Rice, L. M., Simonson, T. & Warren, G. L. (1998). Crystallography & NMR system: a new software suite for macromolecular structure determination. *Acta Crystallog. sect. D,* **54**, 905-921.

Carter, C. W., Jr (1993). Cognition, mechanism, and evolutionary relationships in aminoacyl-tRNA synthetases. *Ann. Rev. Biochem.* **62**, 715-748.

Cavarelli, J., Rees, B., Ruff, M., Thierry, J.-C. & Moras, D. (1993). Yeast $tRNA^{Asp}$ recognition by its cognate class II aminoacyl-tRNA synthetase. *Nature,* **362**, 181-184.

Cavarelli, J., Rees, B., Eriani, G., Ruff, M., Boeglin, M., Gangloff, J., Thierry, J.-C. & Moras, D. (1994). The active site of yeast aspartyl-tRNA synthetase: structural and functional aspects of the aminoacylation reaction. *EMBO J.* **13**, 327-337.

Cusack, S., Berthet-Colominas, C., Härtlein, M., Nassar, N. & Leberman, R. (1990). A second class of synthetase structure revealed by X-ray analysis of *Escherichia coli* seryl-tRNA synthetase. *Nature,* **347**, 249-255.

Delarue, M., Poterszman, A., Nikonov, S., Garber, M., Moras, D. & Thierry, J.-C. (1994). Crystal structure of a prokaryotic aspartyl-tRNA synthetase. *EMBO J.* **13**, 3219-3229.

Dietrich, A., Giegé, R., Comarmond, M.-B., Thierry, J.-C. & Moras, D. (1980). Crystallographic studies on the aspartyl-tRNA synthetase-$tRNA^{Asp}$ system from yeast: the crystalline aminoacyl-tRNA synthetase. *J. Mol. Biol.* **138**, 129-135.

Ebel, J.-P., Giegé, R., Bonnet, J., Kern, D., Befort, N., Bollack, C., Fasiolo, F., Gangloff, J. & Dirheimer, G. (1973). Factors determining the specificity of the tRNA aminoacylation reaction. *Biochimie,* **55**, 547-557.

Ebel, J.-P., Renaud, M., Dietrich, A., Fasiolo, F., Keith, G., Favorova, O., Vassilenko, S., Baltzinger, M., Ehrlich, R., Remy, P., Bonnet, J. & Giegé, R. (1979). Interaction between tRNA and aminoacyl-tRNA synthetase in the valine and phenylalanine system from yeast. In *Transfer RNA: Structure, Properties and Recognition* (Schimmel, P., Söll, D. & Abelson, J., eds), pp. 325-343, Cold Spring Harbor Laboratory Press, Cold Spring Harbor, NY.

Eiler, S., Dock-Brégeon, A.-C., Moulinier, L., Thierry, J.-C. & Moras, D. (1999). Synthesis of aspartyl-$tRNA^{Asp}$ in *Escherichia coli*: a snapshot of the second step. *EMBO J.* **18**, 6532-6541.

Engh, R. A. & Huber, R. (1991). Accurate bond and angle parameters for X-ray protein structure refinement. *Acta Crystallog. sect. A,* **47**, 392-400.

Eriani, G. & Gangloff, J. (1999). Yeast aspartyl-tRNA synthetase residues interacting with $tRNA^{Asp}$ identity bases connectively contribute to $tRNA^{Asp}$ binding in the ground and transition state complex and discriminate against non-cognate tRNAs. *J. Mol. Biol.* **291**, 761-773.

Eriani, G., Delarue, M., Poch, O., Gangloff, J. & Moras, D. (1990). Partition of tRNA synthetases into two classes based on mutually exclusive sets of sequence motifs. *Nature,* **347**, 203-206.

Eriani, G., Prevost, G., Kern, D., Vincendon, P., Dirheimer, G. & Gangloff, J. (1991). Cytoplasmic aspartyl-tRNA synthetase from *Saccharomyces cerevisiae*. Study of its functional organisation by deletion analysis. *Eur. J. Biochem.* **200**, 337-343.

Eriani, G., Cavarelli, J., Martin, F., Dirheimer, G., Moras, D. & Gangloff, J. (1993). Role of dimerization in yeast aspartyl-tRNA synthetase and importance of the class II invariant proline. *Proc. Natl Acad. Sci. USA,* **90**, 10816-10820.

Eriani, G., Cavarelli, J., Martin, F., Ador, L., Rees, B., Thierry, J.-C., Gangloff, J. & Moras, D. (1995). The class II aminoacyl-tRNA synthetases and their active site. Evolutionary conservation of an ATP binding site. *J. Mol. Evol.* **40**, 499-508.

Evans, S. (1993). SETOR: hardware lighted three-dimensional model representations of macromolecules. *J. Mol. Graphics,* **11**, 134-138.

First, E. A. (1998). Catalysis of tRNA aminoacylation by class I and class II aminoacyl-tRNA synthetases. In *Comprehensive Biological Catalysis* (Sinnott, M., ed.), vol. 1, pp. 573-607, Academic Press, New York.

Frugier, M., Florentz, C. & Giegé, R. (1994a). Efficient aminoacylation of resected RNA helices by class II aspartyl-tRNA synthetase dependent on a single nucleotide. *EMBO J.* **13**, 2218-2226.

Frugier, M., Söll, D., Giegé, R. & Florentz, C. (1994b). Identity switches between tRNAs aminoacylated by class I glutaminyl- and class II aspartyl-tRNA synthetase. *Biochemistry,* **33**, 9912-9921.

Frugier, M., Moulinier, L. & Giegé, R. (2000). A domain in the N-terminal extension od class IIb eukaryotic aminoacyl-tRNA synthetase is important for tRNA binding. *EMBO J.* **19**.

Gagnon, Y., Lacoste, L., Champagne, N. & Lapointe, J. (1996). Widespread use of the Glu-tRNA^{Gln} transamidation pathway among bacteria. A member of the α purple bacteria lacks glutaminyl-tRNA synthetase. *J. Biol. Chem.* **271**, 14856-14863.

Giegé, R., Lorber, B., Ebel, J.-P., Moras, D. & Thierry, J.-C. (1980). Cristallisation du complexe formé entre l'aspartate-tRNA de levure et son aminoacyl-tRNA synthétase spécifique. *C. R. Acad. Sc. Paris D2,* **291**, 393-396.

Giegé, R., Frugier, M. & Rudinger, J. (1998a). tRNA mimics. *Curr. Opin. Struct. Biol.* **8**, 286-293.

Giegé, R., Sissler, M. & Florentz, C. (1998b). Universal rules and idiosyncratic features in tRNA identity. *Nucl. Acids Res.* **26**, 5017-5035.

Ibba, M., Sever, S., Praetorius-Ibba, M. & Söll, D. (1999). Transfer RNA identity contributes to transition state stabilization during aminoacyl-tRNA synthesis. *Nucl. Acids Res.* **27**, 3631-3637.

Kleywegt, G. & Jones, A. (1997). Model building and refinement practice. *Methods Enzymol.* **277**, 208-230.

Koradi, R., Billeter, M. & Wuthrich, K. (1996). MOLMOL: a program for display and analysis of macromolecular structures. *J. Mol. Graphics,* **51**, 29-32.

Krauss, G., Riesner, D. & Maass, G. (1976). Mechanism of discrimination between cognate and non-cognate tRNAs by phenylalanyl-tRNA synthetase from yeast. *Eur. J. Biochem.* **68**, 81-93.

Lamour, V., Quevillon, S., Diriong, S., N'guyen, V. C., Lipinski, M. & Mirande, M. (1994). Evolution of the Glx-tRNA synthetase family: the glutaminyl enzyme as a case of horizontal gene transfer. *Proc. Natl Acad. Sci. USA,* **91**, 8670-8674.

Lapointe, J. & Giegé, R. (1991). Transfer RNAs and aminoacyl-tRNA synthetases. In *Translation in Eukaryotes* (Trachsel, H., ed.), pp. 35-69, CRC Press Inc. Boca Raton, FA.

Laskowsky, R. A., McArthur, M. W., Moss, D. S. & Thornton, J. M. (1993). PROCHECK: a program to check the sterochemical quality of protein structures. *J. Appl. Crystallog.* **26**, 283-291.

Lévêque, F., Plateau, P., Dessen, P. & Blanquet, S. (1990). Homology of lysS and lysU, the two *Escherichia coli* genes encoding distinct lysyl-tRNA synthetase species. *Nucl. Acids Res.* **18**, 305-312.

Lorber, B., Giegé, R., Ebel, J.-P., Berthet, C., Thierry, J.-C. & Moras, D. (1983). Crystallization of a tRNA-aminoacyl-tRNA synthetase complex. Characterization and first crystallographic data. *J. Biol. Chem.* **258**, 8429-8435.

Lorber, B., Kern, D., Mejdoub, H., Boulanger, Y., Reinbolt, J. & Giegé, R. (1987). The microheterogeneity of the crystallizable yeast cytoplasmic aspartyl-tRNA synthetase. *Eur. J. Biochem.* **165**, 409-417.

Lorber, B., Mejdoub, H., Reinbolt, J., Boulanger, Y. & Giegé, R. (1988). Properties of N-terminal truncated yeast aspartyl-tRNA synthetase and structural characteristics of the cleaved domain. *Eur. J. Biochem.* **174**, 155-161.

Meinnel, T., Mechulam, Y., Blanquet, S. & Fayat, G. (1991). Binding of the anticodon domain of tRNA$_f^{Met}$ to *Escherichia coli* methionyl-tRNA synthetase. *J. Mol. Biol.* **220**, 205-208.

Meinnel, T., Mechulam, Y. & Blanquet, S. (1995). Aminoacyl-tRNA synthetases: Occurence, structure, and function. In *tRNA: Structure, Biosynthesis, and Function* (Söll, D. & RajBhandary, U., eds), pp. 251-290, Am. Soc. Microbiol. Press, Washington, DC.

Moras, D., Comarmond, M.-B., Fischer, J., Weiss, R., Thierry, J.-C., Ebel, J.-P. & Giegé, R. (1980). Crystal structure of yeast tRNA^{Asp}. *Nature,* **288**, 669-674.

Moulinier, L. (1997). Etude structurale d'un complexe hétérologue aspartyl-ARNt synthétase d'*E. coli*: ARNt^{Asp} de levure, Thèse de l'Université Louis Pasteur, Strasbourg.

Navaza, J. & Saludjian, P. (1997). *AMoRe*: an automated molecular replacement program package. *Methods Enzymol.* **276**, 581-594.

Onesti, S., Miller, A. D. & Brick, P. (1995). The crystal structure of the lysyl-tRNA synthetase (LysU) from *Escherichia coli*. *Structure,* **3**, 163-176.

Otwinowski, Z. & Minor, W. (1997). Processing of X-ray diffraction data collected in oscillation mode. *Methods Enzymol.* **276**, 307-326.

Poterszman, A., Delarue, M., Thierry, J.-C. & Moras, D. (1994). Synthesis and recognition of aspartyl-adenylate by *Thermus thermophilus* aspartyl-tRNA synthetase. *J. Mol. Biol.* **244**, 158-167.

Pütz, J., Puglisi, J. D., Florentz, C. & Giegé, R. (1991). Identity elements for specific aminoacylation of yeast tRNA^{Asp} by cognate aspartyl-tRNA synthetase. *Science,* **252**, 1696-1699.

Qiu, X., Janson, C. A., Blackburn, M. N., Chhohan, I. K., Hibbs, M. & Abdel-Meguid, S. S. (1999). Cooperative structural dynamics and a novel fidelity mechanism in histidyl-tRNA synthetases. *Biochemistry,* **38**, 12296-12304.

Rees, B., Cavarelli, J. & Moras, D. (1996). Conformational flexibilty of tRNA: Structural changes in yeast tRNA^{Asp} upon binding to aspartyl-tRNA synthetase. *Biochimie,* **78**, 624-631.

Rees, B., Webster, G., Delarue, M., Boeglin, M. & Moras, D. (2000). Aspartyl-tRNA synthetase from *Escherichia coli*: flexibility and adaptability to the substrates. *J. Miol. Biol.* **299**, 1157-1164.

Rould, M. A., Perona, J. J., Söll, D. & Steitz, T. A. (1989). Structure of *E. coli* glutaminyl-tRNA synthetase complexed with tRNA^{Gln} and ATP at 2.8 Å resolution. *Science,* **246**, 1135-1142.

Ruff, M., Cavarelli, J., Mikol, V., Lorber, B., Mitschler, A., Giegé, R., Thierry, J.-C. & Moras, D. (1988). A high resolution diffracting crystal form of the complex between yeast tRNA^{Asp} and aspatyl-tRNA synthetase. *J. Mol. Biol.* **201**, 235-236.

Ruff, M., Krishnaswamy, S., Boeglin, M., Poterszman, A., Mitschler, A., Podjarny, A., Rees, B., Thierry, J.-C. & Moras, D. (1991). Class II aminoacyl transfer RNA synthetases: Crystal structure of yeast aspartyl-tRNA synthetase complexed with tRNA^{Asp}. *Science,* **252**, 1682-1689.

Sauter, C., Lorber, B., Kern, D., Cavarelli, J., Moras, D. & Giegé, R. (1999). Crystallogenesis studies on aspartyl-tRNA synthetase: use of phase diagram to improve crystal quality. *Acta Crystallog. sect. D,* **55**, 149-156.

Schimmel, P., Giegé, R., Moras, D. & Yokoyama, S. (1993). An operational RNA code for amino acids and possible relationship to genetic code. *Proc. Natl Acad. Sci. USA,* **90**, 8763-8768.

Schmitt, E., Moulinier, L., Fujiwara, S., Imanaka, T., Thierry, J.-C. & Moras, D. (1998). Crystal structure of aspartyl-tRNA synthetase from *Pyrococcus kodakaraensis* KOD: archeon specificity and catalytic mechanism of adenylate formation. *EMBO J.* **17**, 5227-5237.

Söll, D. & RajBhandary, U. L. (1995). *tRNA: Structure, Biosynthesis, and Function*, Am. Soc. Microbiol. Press, Washington, DC.

Stello, T., Hong, M. & Musier-Forsyth, K. (1999). Efficient aminoacylation of $tRNA^{Lys,3}$ by human lysyl-tRNA synthetase is dependent on covalent continuity between the acceptor stem and the anticodon domain. *Nucl. Acids Res.* **24**, 4823-4829.

Vincendon, P. (1990). Obtention et essais de cristallisation de formes mutées de l'aspartyl-ARNt synthétase cytoplasmique de la levure Saccharomyces cerevisiae, Thèse de l'Université Louis Pasteur, Strasbourg.

Westhof, E., Dumas, P. & Moras, D. (1985). Crystallographic refinement of yeast aspartic acid transfer RNA. *J. Mol. Biol.* **184**, 119-145.

Wolfson, A. D., Khvorova, A. M., Sauter, C., Florentz, C. & Giegé, R. (1999). Mimics of yeast $tRNA^{Asp}$ and their recognition by aspartyl-tRNA synthetase. *Biochemistry,* **38**, 11926-11932.

Zaccaï, G., Morin, P., Jacrot, B., Moras, D., Thierry, J.-C. & Giegé, R. (1979). Interactions of yeast valyl-tRNA synthetase with RNAs and conformational changes of the enzyme. *J. Mol. Biol.* **129**, 483-500.

Edited by R. Huber

(Received 1 February 2000; received in revised form 13 April 2000; accepted 13 April 2000)